The KSS lidar data taken inside the continental shelf is shown in Figures 3 and 4. The data obtained from the unpolarized channel is shown in Figure 3, while both the cross-polarized and copolarized components are shown separately in Figure 4 (the copolarized component was calculated by subtracting the cross-polarized data from the unpolarized data).

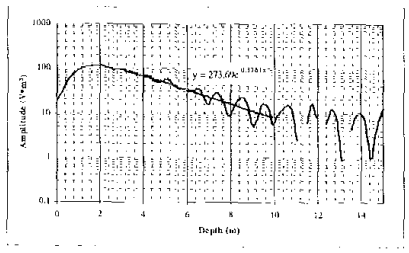

CFI4 Fig. 3. Total KSS lidar return profile obtained from the unpolarized receiver channel inside the continental shelf.

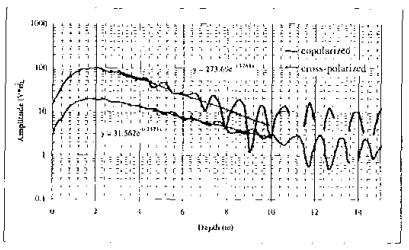

CFI4 Fig. 4. Copolarized and cross-polarized components of the lidar return signal obtained inside the continental shelf.

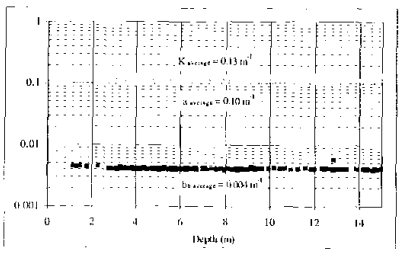

CFI4 Fig. 5. Data obtained from the α-Beta instrument. The diffuse attenuation, K, is shown by triangles, the absorption coefficient, a, is shown by crosses, and the backscatter coefficient, b_b, is shown by squares. Average values of the coefficients are shown above the data points.

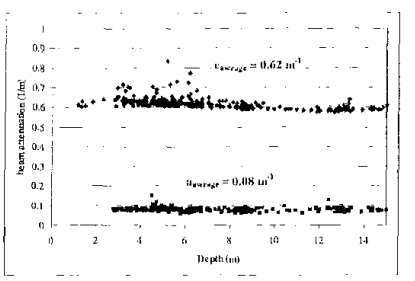

CFI4 Fig. 6. Beam attenuation and absorption data obtained from the AC-9 at λ=532 nm.

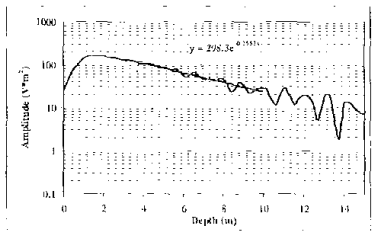

CFI4 Fig. 7. KSS lidar data from the unpolarized receiver channel taken outside the continental shelf.

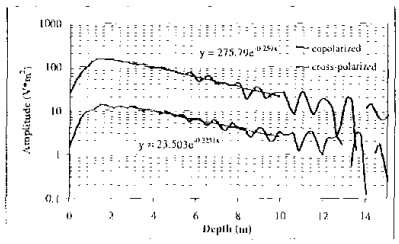

CFI4 Fig. 8. Copolarized and cross-polarized components of the KSS lidar data taken outside the continental shelf.

The system attenuation coefficient for the total lidar return signal in Figure 3 is K_{sys} = 0.188 m^{-1}, which lies between the measured value of the absorption coefficient ($a_{average}$ = 0.16) and the diffuse attenuation coefficient ($K_{average}$ = 0.25 m^{-1}). This result is due to the fact that the receiver field of view and surface viewing area were twice the transmitter beam divergence and spot size. Thus, virtually all of the scattered light was detected and the attenuation was due primarily to absorbed photons.

In Figure 4, the attenuation of the copolarized return signal is identical to that of Figure 3 (K_{sys} = 0.188 m^{-1}), while the cross-polarized attenuation is reduced (K_{sys} = 0.129 m^{-1}). This difference in slope between copolarized and cross-polarized returns is expected when the receiver field of view is large and the water is highly scattering.

The oceanographic data taken outside the continental shelf is shown in Figures 5 and 6. The scattering coefficient was calculated to be b = 0.54 m^{-1}. The diffuse attenuation coefficient, K = 0.13 m^{-1}, classifies this water as Jerlov Type III[1].

DERA Malvern, UK

CFI5 11:15 am

Adaptive optics based on analog parallel stochastic optimization technique

Mikhail A. Vorontsov, Gary W. Carhart, Marc Cohen,* Gert Cauwenberghs* *Army Res. Lab., Information Science and Tech. Directorate, Adelphi, MD 20783*

In this paper we consider both theoretical and experimental aspects of adaptive wavefront phase distortion compensation using direct system performance metric optimization. A brief review of model-free optimization techniques in adaptive optics, with an emphasis on gradient descent methods based on stochastic approximation of the true gradient is presented. The method is extended to include different requirements for wavefront control, as well as information from different wavefront sensor types. It is shown that both can be incorporated into a more general gradient descent optimization paradigm, giving rise to a variety of new control system architectures.

We report on the first experiments with adaptive wavefront correction systems based on simultaneous perturbation stochastic approximation optimization using a VLSI adaptive controller. The VLSI system was used in two different adaptive system configurations: one with a 127-element liquid-crystal phase modulator, and the other with beam steering and 37-channel micromachined deformable mirrors. The sub-millisecond response time of the beam steering and micromachined deformable mirrors, along with fast (up to 1500 iterative steps per second) parallel analog control signal computation using the VLSI system, allowed for adaptive compensation of dynamical laser beam phase aberrations under conditions of strong intensity scintillations.

Johns Hopkins Univ., USA; E-mail: vorontsov@iol.arl.mil

CFI6 11:45 am

A hybrid curvature/Shack-Hartmann wavefront sensor for adaptive optics

C. Paterson, J.C. Dainty, *The Blackett Lab., Imperial College, Prince Consort Road, London, SW7 2BZ, U.K.; E-mail: carlp@ic.ac.uk*

The growing availability and relative low-cost of continuous surface deformable mirrors such as bimorph and electrostatic MEMS membrane mirrors[1] makes them increasingly attractive for adaptive optics (AO) systems, particularly low-cost systems. Both of these mirror types are curvature devices: each actuator input directly controls the curvature of the mirror's surface in front of that actuator. Curvature wavefront sensing[2] is suited to AO systems using these devices, where it can considerably simplify the spatial control of the system, enabling the construction of very efficient systems.

Conventional curvature sensing relies on measuring the intensity in two planes usually at either side of the focal plane[3]: curvature at a position in the wavefront results in differences between the measured intensities at the corresponding positions in the two planes. We propose a method of curvature sensing for AO which relies on measuring the intensity distribution in a single plane. A lenslet array, with each lenslet having an astigmatic component in its phase given by

$$\phi = ar^2\cos(2\theta - \theta_0), \qquad (1)$$

is used to produce a set of astigmatic foci. The structure of each focal spot is dependent on the curvature of the wave at the lenslet aperture, which can be used to give a curvature signal from a quad-cell detector placed at the focus[4] (see figure 1). The curvature signal is

$$s_c = \frac{(s_1 + s_3) - (s_2 + s_4)}{s_1 + s_2 + s_3 + s_4}. \qquad (2)$$